

<https://doi.org/10.1038/s42005-024-01747-x>

Anomalous quantum transport in fractal lattices

Check for updates

Abel Rojo-Francàs^{1,2,3}, Priyanshu Pansari⁴, Utso Bhattacharya^{5,6}, Bruno Juliá-Díaz^{2,3} & Tobias Grass^{1,7} ✉

Fractal lattices are self-similar structures with repeated patterns on different scales. Quantum transport through such structures is subtle due to the possible co-existence of localized and extended states. Here, we study the dynamical properties of two fractal lattices, the Sierpiński gasket and the Sierpiński carpet. While the gasket exhibits sub-diffusive behavior, sub-ballistic transport occurs in the carpet. We show that the different dynamical behavior is in line with qualitative differences of the systems' spectral properties. Specifically, in contrast to the Sierpiński carpet, the Sierpiński gasket exhibits an inverse power-law behavior of the level spacing distribution. As a possible technological application, we discuss a memory effect in the Sierpiński gasket which allows to read off the phase information of an initial state from the spatial distribution after long evolution times. We also show that interpolating between fractal and regular lattices allows for flexible tuning between different transport regimes.

Recent advances in the engineering of quantum systems have spurred quantum technology applications, including the vast field of quantum simulation. Different experimental platforms allow for the design and control of completely artificial quantum systems, with or without real-world counterpart. Recent examples for a simulation setup exploring the laws of quantum physics beyond standard geometries are quantum particles in fractal lattices, including electronic systems generated by molecular assembly¹ or using scanning tunneling microscopy², photonic systems of coupled optical fibers^{3,4}, or cold atoms in optical tweezers⁵. In general, fractal lattices are characterized by self-similar patterns repeated on different scales which give rise to a fractal Hausdorff dimension⁶. In the present article, we concentrate on Sierpiński fractals, specifically the Sierpiński gasket and the Sierpiński carpet. The self-similar construction scheme for these fractals is illustrated in Fig. 1a, b. The fractal (Hausdorff) dimension of these structures is $d_f = \log(3)/\log(2) \approx 1.585$ for the gasket, and $d_f = \log(8)/\log(3) \approx 1.893$ for the carpet⁷. Exploring how the fractal geometry affects the dynamical behavior of quantum systems is an interesting research endeavor, and fascinating effects are found already in the single-particle domain: For instance, the combination of non-standard fractal geometry and topology has attracted significant interest^{8–13}. The fate of topological edge states in fractal lattices, where a true bulk is absent, has now been studied experimentally using photonic waveguide arrays⁴. Also in the absence of topological features, the

transport in fractal lattices is a rich research subject. In general, transport behavior can be characterized through the mean square distance $\text{MSD}(t)$ from the initial position, and in particular, through its scaling as a function of time:

$$\text{MSD}(t) \sim t^\alpha. \quad (1)$$

Transport is called sub-diffusive for $\alpha < 1$, diffusive for $\alpha = 1$, super-diffusive or sub-ballistic for $1 < \alpha < 2$, ballistic for $\alpha = 2$, hyper-ballistic for $\alpha > 2$. Classical diffusion on fractals has been studied extensively since the 1980s^{14–18}, and sub-diffusive behavior with $\alpha = d_s/d_f$ has been established, where d_s is the spectral dimension. In contrast to the fractal dimension d_f , the spectral dimension d_s takes into account also the connectivity of the fractal lattice. It has a universal value, $d_s = 4/3$, at percolation threshold according to the Alexander-Orbach conjecture¹⁵. For Sierpiński fractals, the values $d_s = 2 \log(3)/\log(5) \approx 1.365$ and $d_s \approx 1.805$ have been obtained for gasket and carpet¹⁹, respectively. Random fractals allow for independently tuning Hausdorff and spectral dimension, and the latter has been found most relevant also in the context of quantum transport²⁰. Quantum-mechanical transport in the Sierpiński gasket has been contrasted to the classical random walk in ref. 19. Studying the return probability of a quantum object evolving in the Sierpiński gasket, it has been shown that, instead of the

¹DIPC - Donostia International Physics Center, San Sebastián, Spain. ²Departament de Física Quàntica i Astrofísica, Facultat de Física, Universitat de Barcelona, Barcelona, Spain. ³Institut de Ciències del Cosmos, Universitat de Barcelona, ICCUB, Barcelona, Spain. ⁴Indian Institute of Technology, Roorkee, India. ⁵ICFO - Institut de Ciències Fotòniques, The Barcelona Institute of Science and Technology, Castelldefels, Barcelona, Spain. ⁶Institute for Theoretical Physics, ETH Zurich, Zurich, Switzerland. ⁷IKERBASQUE, Basque Foundation for Science, Bilbao, Spain. ✉ e-mail: tobias.grass@dipc.org

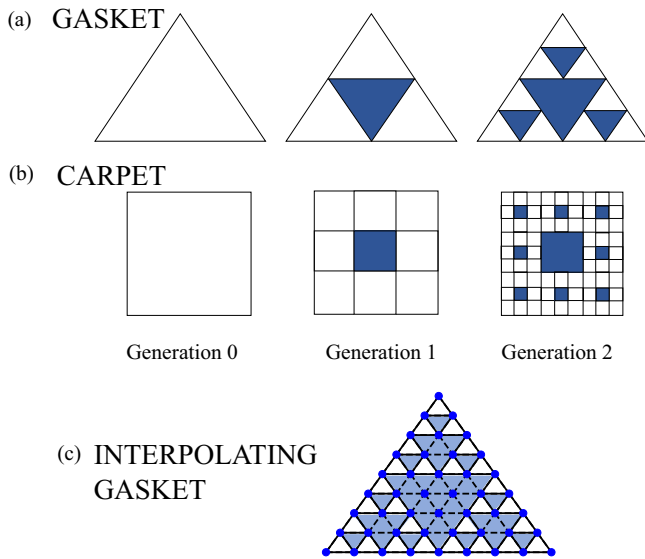


Fig. 1 | Construction scheme for fractal lattices. a Sierpiński gasket and (b) Sierpiński carpet, showing in white the region of the fractal structure and in blue the regions that do not belong to the fractal. In (c) we show a lattice, where the solid lines form a 3rd generation Sierpiński gasket, and the dashed lines interpolate between the fractal gasket and a regular triangular lattice.

classical decay $t^{-d_s/2}$, the quantum return probability in the Sierpiński gasket oscillates and remains above the classical value at all times. Notably, such a behavior is not apparent in the (finite-size) Sierpiński carpets, also studied in ref. 19, hinting for different transport behavior of these two fractal structures. In ref. 21, quantum transport in Sierpiński carpets has been under scrutiny, also reporting clear differences between carpet and gasket. While in the Sierpiński gasket conductance is zero in extended energy regions, this is not the case in the Sierpiński carpet. As a possible geometric reason for this difference ref. 21 mentions the infinite ramification number of the Sierpiński carpet²², in contrast to a finite ramification number in the Sierpiński gasket. The ramification number counts the number of bonds that have to be cut in order to separate different iterations of the fractal. The increased quantum return probability in the Sierpiński gasket can be seen as a dynamical consequence of the existence of localized eigenstates. Localized states in the Sierpiński gasket have first been found in ref. 23 using the Migdal-Kadanoff decimation technique. In fact, this early work had conjectured that *all* quantum states in the Sierpiński gasket are exponentially localized, considering its spectral similarities to 1D quasi-crystals^{24,25}, and the fact that, like in disordered media or in quasi-crystals, the absence of Bloch’s theorem can give rise to quantum interference effects which slow down the dynamics of a quantum object and possibly lead to Anderson localization²⁶. However, later work²⁷ has shown that the Sierpiński gasket exhibits a more complex behavior, as in addition to the localized states also an infinite number of extended states were found to live on the gasket. Recently, quantum transport in fractal geometries has been explored also experimentally in ref. 3, reporting super-diffusive quantum transport through Sierpiński gasket and carpet, with the scaling exponent $\alpha = d_f$ given by the fractal (Hausdorff) dimension of the lattice. Although these values are smaller than the ballistic diffusion exponent, $\alpha = 2$, obtained for quantum diffusion on planar Bravais lattices^{28,29}, they still constitute a significant quantum speed-up on fractals, in contrast to the increased return probability reported in ref. 19 and the expected quantum localization effect. Given this controversial assessment on the transport behavior in Sierpiński fractals, the present manuscript revisits this scenario. For the gasket, we show that tiny changes in the connectivity of the lattice switch the particle’s transport behavior from the super-diffusive motion reported in ref. 3 to a sub-diffusive one, with a quantum transport exponent $\alpha \approx 0.73$ that is smaller than the classical value $\alpha = d_s/d_f \approx 0.86$, in line with the point of view

of Anderson localization. On the other hand, for the carpet, our study confirms super-diffusive behavior with $\alpha \approx 1.8$. This surprising difference between the two structures can be understood from their different spectral properties, already noted in ref. 19. Specifically, for the Sierpiński gasket, a relation is established between α and the exponent of an inverse power-law scaling of the level spacing distribution. The stark contrast between sub-diffusive transport on the Sierpiński gasket and ballistic behavior on the regular lattice, together with the tunability of synthetic quantum lattices, opens an avenue to freely tune the transport behavior through all regimes by interpolating between the fractal lattice and the regular lattice, as illustrated in Fig. 1c. In addition to this opportunity, we also discuss a memory effect in dynamics of the Sierpiński gasket, which possibly may lead to applications as a quantum memory. Specifically, we demonstrate that the localized quantum dynamics on the Sierpiński gasket does not only significantly slow-down the spreading of a wave packet, but it also keeps memory of relatively fragile quantities like the phase of a quantum superposition. To this end, we compare the evolution of non-classical states, specifically symmetric and anti-symmetric arrangement of a delocalized object, and we find that the anti-symmetric superposition experiences slower initial spreading due to quantum interference. Interestingly, this leads to significantly different MSD(t) values even at long times, when in a regular lattice initial differences have been washed out.

Results

Quantum transport on Sierpiński fractals

We start by considering the mean square distance of a particle on the Sierpiński gasket which is initially prepared in one of the corners. An explicit definition of the tight-binding model is given in the Methods section. For different generations of the fractal, the obtained behavior is shown in Fig. 2a. Each of these curves can be divided into three temporal regimes:

- Short times, $tJ \lesssim 1$: Ballistic regime. On short times, the system behaves ballistically, $\text{MSD}(t) \sim t^\alpha$ with $\alpha \approx 2.1$. In this regime the system has yet no notion of the fractal geometry, and the behavior is the same as in a regular lattice. We note that the slightly hyper-ballistic value of $\alpha > 2$ is a consequence of preparing the state near the boundary. For such initial conditions, also regular lattices exhibit the same increased value of α .
- Intermediate times, $1 \lesssim tJ \lesssim TJ$ with $T = (L/a)^{d_f}/(4J)$: Sub-diffusive regime. On intermediate-times, the system behaves sub-diffusively, with $\alpha \approx 0.56$. The extent of this regime is limited by the system size, determined by the fractal dimension d_f and the side length L of the triangle. We note again that also in this regime the exact value of α depends on the initial conditions, as we further discuss below.
- Long times, $t \gtrsim T$: Quasi-localized regime. The evolution of the MSD(t) flattens further and becomes extremely slow. On long time scales, the behavior can be described on average with an exponent $\alpha \lesssim 0.15$, cf. Fig. 2b.

It is important to note that at $t \approx T$, i.e., at the transition from the intermediate regime to the long-time regime, MSD(T) is still far below its thermalized value. In a thermalized system, the center of mass of the wave function would be at the center of the triangle, hence for a system initially prepared in one of the corners, the square distance between the corner and the center of the triangle defines the thermalized value, $\text{MSD}_{\text{th}} = L^2/3$. With the intermediate regime being too short to thermalize the system and with the subsequent evolution being extremely slow, it turns out that in the Sierpiński gasket the thermalized value will essentially never be reached. This can be seen from Fig. 2b which extends up to $tJ = 10^6$, i.e., to times scales which are clearly beyond experimentally realistic values. Even on this time scale, the MSD remains below 1000 for a system with $L = 128$, that is $\text{MSD}_{\text{th}} = 5461$. Of course, this example does not exclude the possibility of thermalization on even longer time scales which then become difficult to assess even in a numerical simulation due to the numerical precision. However, it is possible to argue rigorously that in the thermodynamic limit the system will not thermalize. Therefore, we note that MSD(T) scales sub-linearly with the system size, $\text{MSD}(T) \sim T^\alpha \sim L^{0.56d_f}$, in contrast to the quadratic size dependence of

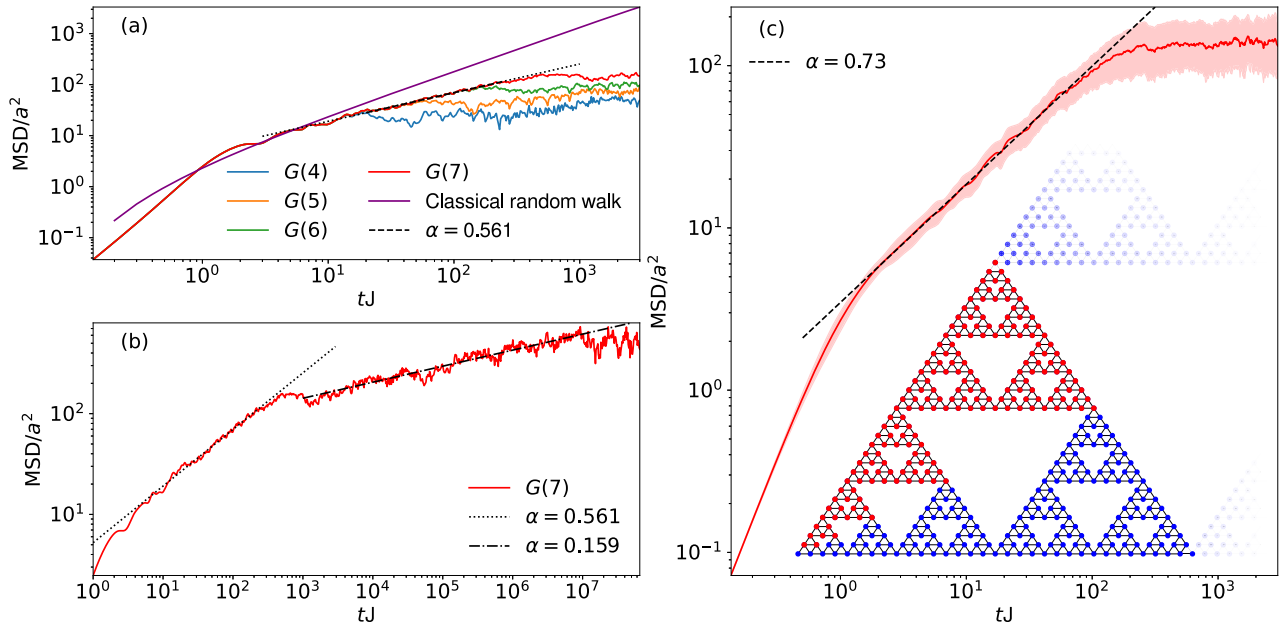


Fig. 2 | Mean square distance for Sierpiński gasket. **a** Mean square distance $MSD(t)$ of a particle starting from one corner of a Sierpiński gasket of generation $G(X)$ with $X = 4, 5, 6, 7$. This corresponds to $D = 123, 366, 1095, 3282$ sites, or triangles of length $L = 16, 32, 64, 128$. On time scales up to $t \sim 1/J$, the particle behaves ballistically, $MSD(t) \sim t^\alpha$ with $\alpha \approx 2.1$. On an intermediate time scale bound by the system size, the system evolves sub-diffusively, with an exponent $\alpha = 0.561 \pm 0.005$. Beyond that regime, the $MSD(t)$ almost flattens. The value reached at that time is still far away from the center of the triangle, $MSD \ll L^2/3$. For comparison, we also plot the MSD of a classical continuous-time random walk on a $G(7)$ gasket. **b** Same plot as in

(a) for the 7th generation of the Sierpiński gasket, but on an extremely long time scale. We extract a long-time scaling $\alpha = 0.159 \pm 0.003$ from this figure. **c** For the 6th generation Sierpiński gasket, we analyze the behavior of $MSD(t)$ averaged over a set of different initial positions, as indicated by the red-colored sites, together with a standard deviation of the averaged $MSD(t)$. In the intermediate temporal regime, we find $\alpha = 0.73 \pm 0.01$. J is the hopping term between each connected site and a is the distance between neighbor sites. The errors on the exponent α are associated with the fit parameters error.

$MSD_{th} \sim L^2$. Hence, for larger systems the difference to a thermalized state gets more and more enhanced.

So far we have studied only the transport starting from a very special initial state where the particle is prepared in one corner of the triangle. However, in contrast to the case of an (infinite) Bravais lattice, the fractal lattice has non-equivalent lattice sites, and hence, the choice of initial state may affect the dynamical behavior. Indeed, when considering initial preparation on a variety of different sites, see Fig. 2c, the exponent α in the intermediate regime tends to be larger for generic initial states as compared to an initial corner state. While the dynamics remains sub-diffusive for all initial states which we have considered, the $MSD(t)$ averaged over different initial states, plotted in Fig. 2c together with its standard deviation, evolves with an exponent $\alpha \approx 0.73$.

The behavior on the Sierpiński gasket is in stark contrast to the quantum diffusion in a regular triangular structure. In that geometry, the ballistic initial behavior (with the possibility of $\alpha > 2$ due to preparation near the boundary) is maintained up to a saturation time $T' \sim L^2$ at which the system enters a thermalized regime with $MSD(t)$ oscillating around MSD_{th} .

The behavior on the Sierpiński gasket is also very different from the dynamics on the Sierpiński carpet. Instead of sub-diffusive transport, the carpet exhibits a highly super-diffusive, or sub-ballistic behavior, with $\alpha \approx 1.8$, see Fig. 3. This value is similar to the one previously obtained in ref. 3, and it constitutes a significant quantum speed-up, compared to the classical value $\alpha = d_s/d_f \approx 0.95$. In this context, it should be noted that even for some non-Bravais periodic lattices sub-ballistic quantum transport has been found, e.g., with a value of $\alpha \approx 1.71$ for the honeycomb lattice²⁹.

The sub-diffusive dynamics observed here at intermediate times in the Sierpiński gasket is in contrast to the super-diffusive behavior reported in ref. 3, with $\alpha \approx 1.59$. The origin of this discrepancy is a subtle difference in the definition of the fractal lattice: while the setup of ref. 3 incorporates tunneling between any pair of nearest-neighbor sites, the lattice studied in the

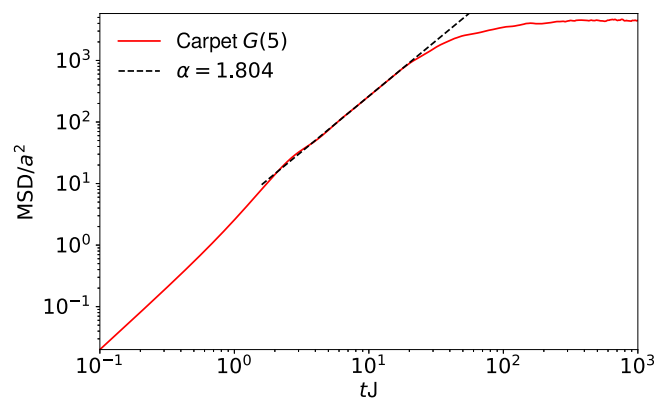


Fig. 3 | Mean square distance for Sierpiński carpet. For a fifth generation $G(5)$ Sierpiński carpet lattice, we show the mean square distance $MSD(t)$ as a function of time. The initial state is conformed by a particle on a corner of the lattice and evolves freely. There is a fit region with slope $\alpha = 1.804 \pm 0.001$. J is the hopping term between each connected site and a is the distance between neighbor sites. The error on the exponent α is associated with the fit parameters error.

present work has the connectivity which is shown in Fig. 2c. Here, hopping processes occur only between nearest neighbors belonging to the same generation of the fractal. In this case, the three corner sites of each generation are obvious bottlenecks, as different generations are connected only via these sites. The remarkably different transport behavior on the two graphs, which are both characterized by the same Hausdorff dimension, suggest that the dynamics is crucially influenced by the ramification properties of the graph. Although both structure are finitely ramified, incorporating nearest-neighbor links between pairs from different generations doubles its ramification number.

Spectral properties on the Sierpiński gasket

Quite generally it is known from random matrix theory that the spacing between adjacent energy levels provides deep insight into the dynamical behavior of a quantum system³⁰. Specifically, ergodic systems exhibit level repulsion, and their level spacing distribution $p(s)$ has a power-law behavior $p(s) \sim s^\beta$ for $s \rightarrow 0$. This allows for classifying the system according to the exponent β . For the energy spectrum in fractal lattices, similarly to the case of quasi-crystals, level spacing analysis seems, on first sight, to be inappropriate, since the energy spectrum is characterized by huge degeneracies³¹. However, in refs. 32–34, the concept of level spacing distribution has been adapted to the highly degenerate Cantor spectrum of quasi-periodic 1D models, and an inverse power law $p(s) \sim s^{-\beta}$ has been found. To test this behavior, the integrated level spacing distribution $p_{\text{int}}(s) = \int_s^\infty ds' p(s')$ can be considered, by counting the number of gaps larger than s . In a finite system, this leads to a devil's staircase which, due to self-similarity of the spectrum across various scales, can be smoothed to a power law,

$$p_{\text{int}}(s) \sim s^{1-\beta}. \tag{2}$$

The exponent β of the level spacing distribution and the exponent α of the mean square distance can be related in the following way^{32,34}: By definition of the integrated level spacing distribution, the number of states which can be energetically resolved with an energy resolution s (in units of the hopping energy $\hbar J$) is given by $p_{\text{int}}(s) \sim s^{1-\beta}$. On the other hand, considering that the volume of a system scales with length L (in units of the lattice constant a) as L^{d_f} , where d_f is the Hausdorff dimension, we also have $L^{d_f} \sim p_{\text{int}}(s)$. Hence, the smallest energy resolution s is related to the length L of the system as $L \sim s^{(1-\beta)/d_f}$. At the same time, the relation $\text{MSD} \sim t^\alpha$ connects a largest length scale L to a largest time scale t (in units $1/J$) via $L \sim t^{\alpha/2}$, or alternatively, to a smallest energy scale $s \sim t^{-1}$ via $L \sim s^{-\alpha/2}$. Combining these scaling relations leads to

$$\alpha = \frac{2(\beta - 1)}{d_f}. \tag{3}$$

Here, we analyze the spectral properties of different geometries by plotting the integrated level spacing distribution, $p_{\text{int}}(s)$, that is, the (normalized) number of energy gaps larger than s , see Fig. 4. Indeed, for the Sierpiński gasket we find that within an extended region in energy, the staircase function is approximated by an inverse power law, $p_{\text{int}}(s) \sim s^{1-\beta}$, as seen by using a double-logarithmic axis scale. Numerically, we obtain $\beta = 1.6 \pm 0.05$. The proximity of β to the Hausdorff d_f seems suggestive that both quantities might be identical, but we are lacking any a priori argument for such a relation. Importantly, the fractal dimension relates β to α through Eq. (3), and for $\beta = 1.60 \pm 0.05$, we expect $\alpha = 0.76 \pm 0.06$, in accordance with the α obtained before by averaging over different initial states.

For other geometries than the with Sierpiński gasket, the integrated level spacing distribution is qualitatively different: Neither a regular lattice with triangular or square geometry, nor the Sierpiński carpet exhibits an extended spectral regime which can be approximated by an inverse power-law, see Fig. 4. As we have argued above, both the Sierpiński carpet and regular lattices (square or triangular) exhibit much faster transport behavior than the Sierpiński gasket, within or close to the ballistic regime. In this context, the Sierpiński gasket of the experiment in ref. 3 appears to be an intermediate case: For sufficiently large gaps, the level spacing distribution, shown in green in Fig. 4, can still be approximated by power-law scaling. The exponent is found to be significantly larger than in the case of a standard Sierpiński gasket, $\beta = 2.25 \pm 0.05$. It is noted that, by applying Eq. (3), this value of β is in full agreement with the exponent $\alpha \approx 1.59$ of the MSD scaling, reported in ref. 3.

Transport on interpolating lattices

The very different transport behavior of Sierpiński gasket and regular triangular lattice open up a route to tailor-made transport behavior by interpolating between these two cases, as sketched in Fig. 1c. The interpolating

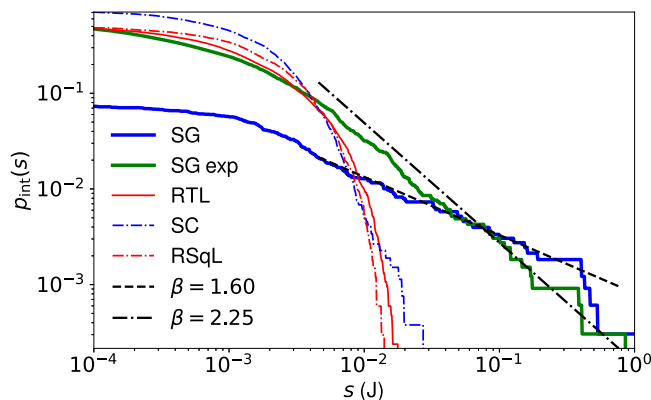


Fig. 4 | Energy gaps distribution. Integrated level spacing distribution $p_{\text{int}}(s)$ for the energy spectra on different lattices: Solid lines are for triangular geometries, with the fractal Sierpiński gasket (SG) of generation 7 (3282 sites) in blue, the corresponding regular triangular lattice (RTL) with 8385 sites in red, and the Sierpiński gasket used in experiment³ in green (SG exp.) The dash-dotted lines correspond to square geometries, where the blue is the fractal Sierpiński carpet (SC) of generation 5 (5280 sites), and the red one is the regular square lattice (RSqL) with the same basis (6724 sites). Only on the gasket (SG and SG exp), the integrated level spacing distribution exhibits approximately an inverse power-law behavior $p_{\text{int}}(s) \sim s^{1-\beta}$. This allows to determine the exponent β via fitting, $\beta \approx 1.60 \pm 0.05$ for SG, and $\beta \approx 2.25 \pm 0.05$ for SG exp.

lattice contains all sites of the regular lattice, but for the bonds at those sites which are exclusive to the regular lattice a different hopping amplitude J' is chosen (as compared to the hopping amplitude J on the fractal). In Fig. 5a, the $\text{MSD}(t)$ is plotted for various interpolating choices $\gamma \equiv J'/J$. Also in the intermediate case (i.e., $0 < J' < J$), the transport behavior can be separated into three temporal regimes. Our main interest is the exponent α for the intermediate temporal regime, in between the dashed lines of Fig. 5a. We plot this value α in Fig. 5b, showing that the transport properties can continuously be tuned from the sub-diffusive regime in the fractal lattice $\gamma \lesssim 0.3$, through a super-diffusive regime ($0.3 \lesssim \gamma \lesssim 0.8$), into a ballistic regime in the (almost) regular lattice ($\gamma \gtrsim 0.8$).

Role of disorder

We have also studied the effect of a disorder potential $V_d \mu_i$ on each site i , where V_d is the disorder strength, and μ_i random numbers between 0 and 1, drawn from a uniform distribution $U(0,1)$. In Fig. 6a, we show the evolution of the MSD for a particle prepared in one corner of the fifth generation Sierpiński gasket for different V_d , averaged over 100 disorder realizations. For weak disorder, the evolution is essentially unchanged by the disorder potential, except for a smoothing effect which is due to the disorder averaging, and which sets in after a time scale that depends on the disorder strength. This finding is particularly relevant from the point of view of experiments, because it shows that unavoidable weak disorder does not alter the dynamical behavior. From a theoretical point of view, it is interesting to see that very strong disorder ($V_d \gg J$) further slows down the dynamics and leads to a saturation of the MSD at a smaller value than in the clean gasket. In Fig. 6b we also plot the MSD at long times as a function of V_d . Strong enough disorder leads to an exponential decay of the long-time MSD. For an interpretation of this observation, we note that low-dimensional systems (i.e., 1D or 2D systems) are known to localize at any disorder strength, with a localization length which depends on the disorder strength, and which for weak disorder may exceed the size of a finite system. The behavior seen in the Sierpiński gasket is interpreted as a competition between two different localization mechanisms: For weak disorder, the localizing effect of the fractal structure is dominant, and we do not observe an effect due to the disorder. Strong disorder, in contrast, produces a localization length that confines the dynamics in a stronger way than the fractal structure. In this case, the effect of disorder becomes apparent in the system evolution.

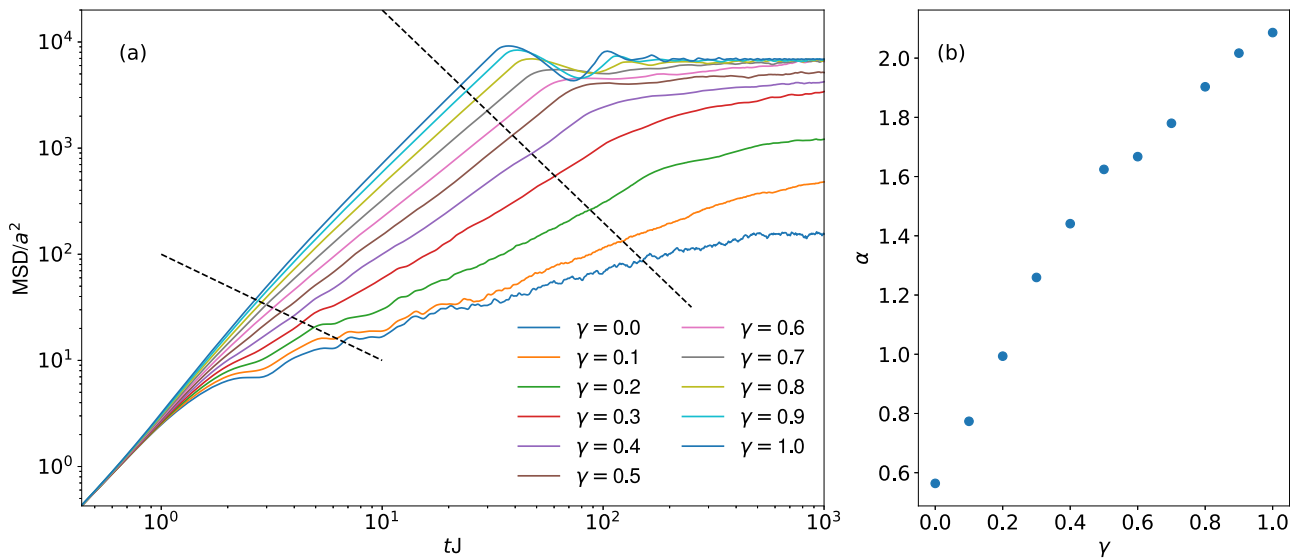


Fig. 5 | Interpolate Sierpiński gasket. **a** Mean square distance $MSD(t)$ of a particle in an interpolating lattice, cf. Fig. 1c, characterized by the ratio $\gamma \equiv J'/J$ between hopping parameters J' exclusive to the regular lattice, and J in both regular and fractal lattice. We initialize the evolution in one corner of an interpolating gasket of generation 7. The slowest behavior is obtained in a fully fractal geometry ($\gamma = 0$), whereas the fastest behavior corresponds to regular triangular lattice ($\gamma = 1$). **b** For

the different values of γ , we extract the exponent α of the mean square distance (from fits to the curves in (a) in the intermediate regime marked by the dashed lines). The result is plotted as a function of γ . The error bars of the fitted α are smaller than the circles displayed. a is the distance between neighbor sites.

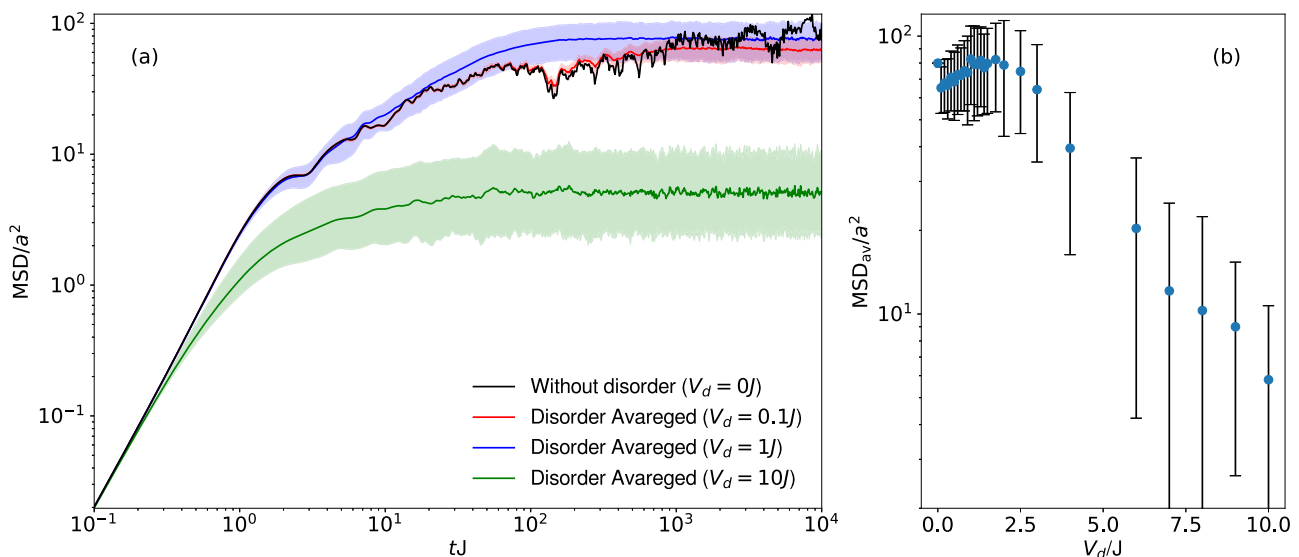


Fig. 6 | Disordered Sierpiński gasket. **a** Mean square distance $MSD(t)$ of a particle starting from one corner of a Sierpiński gasket of generation $G(5)$ for different disorder strengths V_d . The solid lines correspond to the average over 100 random configurations whereas the colored region is the standard deviation. **b** Mean square distance for long times MSD_{av} obtained by averaging the MSD from $tJ = 10^3$ to

$tJ = 10^4$, as a function of the strength of the random potential V_d with the error bars obtained with the standard deviation. J is the hopping term between each connected site and a is the distance between neighbor sites.

Discussion

Our results have established that the dynamics on the Sierpiński gasket is coined by the localized eigenstates and an inverse-power-law level spacing distribution, in stark contrast to the case of regular lattices or Sierpiński carpet. We now discuss how this localized nature of the gasket leads to a memory effect which possibly might be used as a quantum memory. Clearly, the slow growth of the $MSD(t)$ and the demonstrated inability of reaching a thermalized value keep memory of the classical information about the initial position of the

particle. This is also illustrated in Fig. 7, showing that after initial preparation in the corner of a $G(7)$ gasket, the weight of the time-evolved wave function will remain concentrated in the surrounding $G(1)$ gasket (indicated in blue). Considering the surrounding $G(6)$ structure, i.e., roughly 1/3 of the total lattice, this will keep more than 95 % of the weight for all times. In contrast, for the case of a regular lattice we see a rapid drop to the thermalized value 1/3.

Importantly, the Sierpiński gasket is also able to memorize quantum properties of the initial state. To this end, we consider the initial quantum

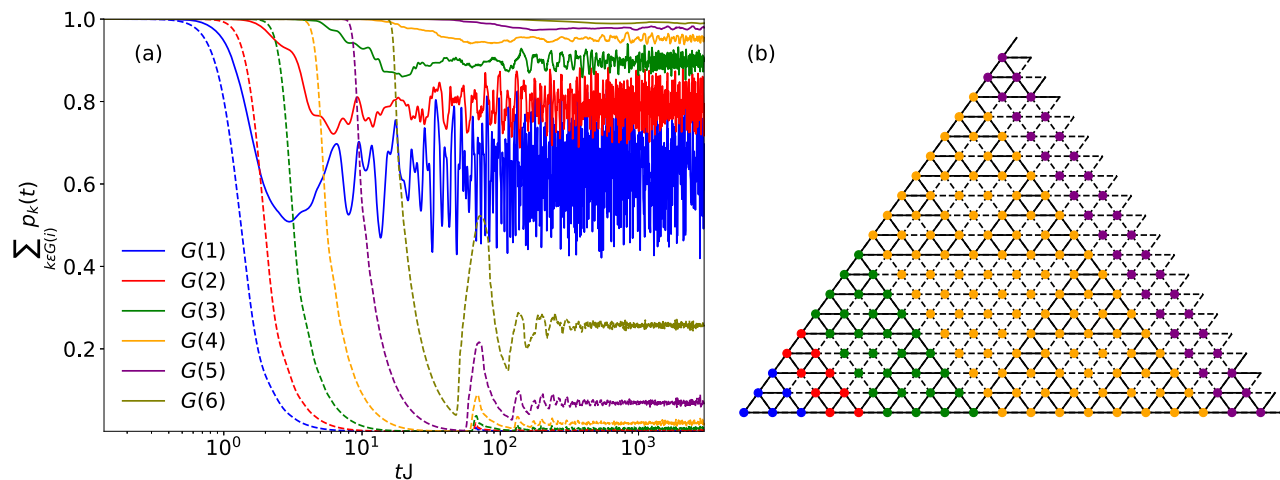


Fig. 7 | Localization on fractal lattice. After preparing the system initially in the lower left corner of a G(7) Sierpiński gasket or the corresponding regular triangle, we plot in (a) the weight of the wave function within the lower-leftmost G(*i*) structure (as indicated in (b)). In the regular lattice the weight decays quickly and thermalizes

at the thin dashed lines, corresponding to the ratio of site numbers $N_s[G(i)]/N_s[(G7)]$. In contrast, the weight in the fractal (solid lines), will always keep some memory of the initial state. *J* is the hopping term between each connected site.

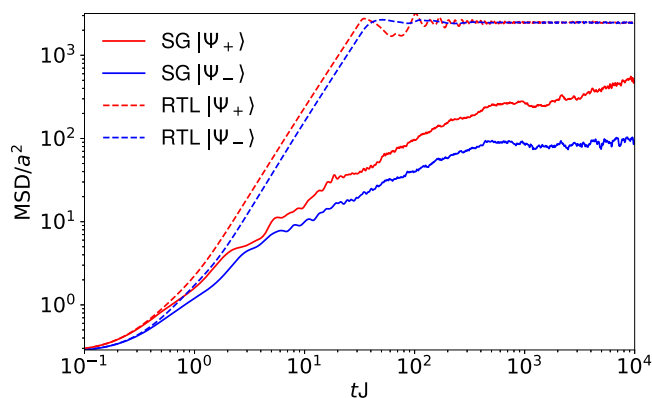


Fig. 8 | Non-classical initial state. Mean square distance $MSD(t)$ of a particle with a non-classical initial state. The particle is prepared in a superposition of being in the corner and one of its first neighbors. The solid red line corresponds to a particle in a seventh generation Sierpiński gasket with a symmetric initial configuration. The solid blue line corresponds to the anti-symmetric initial condition for the fractal geometry. The dashed lines correspond to a standard triangular lattice geometry with the same basis as the fractal considered. *J* is the hopping term between each connected site and *a* is the distance between neighbor sites.

superposition

$$|\Psi_{\pm}\rangle = \frac{1}{\sqrt{2}}(|A\rangle \pm |B\rangle), \tag{4}$$

with + denoting the symmetric, and – the anti-symmetric superposition. The states $|A\rangle$ and $|B\rangle$ denote two different initial positions, where for concreteness we choose $|A\rangle$ to be a corner state and $|B\rangle$ its neighbor. Defining $MSD(t)$ with respect to their center-of-mass, we find that the anti-symmetric state $|\Psi_{-}\rangle$ evolves slower as compared to the symmetric state $|\Psi_{+}\rangle$, see Fig. 8. We attribute this difference to destructive interference effects during the simultaneous tunneling from *A* and *B* to their common neighbor. Such a confinement effect stemming from the phase of the wave function is also found initially on a regular lattice. However, on longer time scales only the fractal lattice keeps memory of the initial phase difference in form of a significantly different $MSD(t)$. In the regular lattice, as can also be seen from Fig. 8, both initial states evolve to

the same MSD_{th} , and there is no obvious indicator of the initial phase difference.

If we interpret the two states of Eq. (4) as a qubit, and consider the presence of slow dephasing noise, it is clear that the information of this qubit will be lost with time. However, as we have shown, the evolution in the fractal lattice encodes the information in the spatial distribution of the wave function, and thereby provides some robustness against dephasing noise. We speculate that this might be exploited as some form of quantum memory.

In future work, it will be interesting to explore this effect beyond single-particle physics. For example, one could consider two or more entangled particles evolving quantum-dynamically but under the influence of a certain measurement rate. We expect that the measurement-induced entanglement transition³⁵ will depend on the geometry, and the Sierpiński gasket will maintain the entanglement at higher measurement rates as compared to regular lattices or the Sierpiński carpet. These investigations are also relevant to further advance our idea of using quantum particles in the Sierpiński gasket as quantum memory. In the many-body regime, we expect to find a glass and/or many-body localized phase in the Sierpiński gasket, whereas such a phase is not expected on the carpet. In view of the computational complexity of quantum many-body physics and open quantum systems, we expect that quantum simulations with interacting particles on fractal lattices will be particularly useful and provide important new insights into exotic quantum phenomena. This may include electronic and atomic fractal systems, cf. refs. 1,2,5, or by adding optical non-linearities to the photonic simulations. In particular in the context of electronic materials, it will also be relevant to study the effect of finite temperature which might produce a crossover between quantum transport and the classical random walk scenario. So far, theoretical attempts to study quantum many-body phases in fractal lattices include studies of quantum phase transitions and quantum criticality in interacting spin models^{36–38}, the study of interacting topological systems, in particular with respect to the fate of anyons^{39–41}, or the very recent mean-field study of the Bose-Hubbard model on the Sierpiński gasket⁴².

Methods

Quantum transport

We study tight-binding systems described by a Hamiltonian of the form

$$H/\hbar = - \sum_{ij} J_{ij} a_i^\dagger a_j + \sum_i \epsilon_i n_i. \tag{5}$$

Our focus is on fractal lattices, in particular the Sierpiński gasket and Sierpiński carpet, where sites i are the vertices of the structure. The construction scheme for these fractals is illustrated in Fig. 1a, b. The tunneling amplitude $J_{ij} = J\delta_{\langle i,j \rangle}$ is non-zero between nearest-neighbors within each generation of the fractal. We note that on the Sierpiński gasket there are also nearest-neighbor pairs where the sites belong to different generations of the fractal. While tunneling between these sites is possible in the experimental realization of ref. 3, we have set J_{ij} to zero along these links. We have also studied the case of an interpolating lattice, as shown in Fig. 1c, where we have nearest-neighbor hopping on a regular lattice, but with two types of couplings, J belonging to the Sierpiński fractal, and J' for the others. The on-site frequencies ϵ_i are, where not otherwise defined, homogeneous, $\epsilon_i = \epsilon$. With this choice, the diagonal term of the Hamiltonian is proportional to the identity matrix and only contributes an irrelevant overall phase factor. Hence, we choose $\epsilon = 0$. By numerical diagonalization of (H/\hbar) , we find the eigenvectors $|\alpha\rangle$ and eigenvalues ω_α of the tight-binding model on finite lattices, which then allows us to evolve an arbitrary initial state $|\Psi(0)\rangle$ to time t ,

$$|\Psi(t)\rangle = \sum_{\alpha} \langle \alpha | \Psi(0) \rangle e^{-i\omega_{\alpha}t} |\alpha\rangle. \quad (6)$$

We are then interested in different observables which are best defined in a local basis $|i\rangle = a_i^{\dagger}|\text{vac}\rangle$, that is, a basis of states where the particle exclusively occupies one site i . Specifically, the probability to be at a given site i at time t reads $p_i(t) = |\langle i | \Psi(t) \rangle|^2$. If the particle has initially been prepared at a site i , i.e., $|\langle i | \Psi(0) \rangle| = 1$, the quantity $p_i(t)$ equals the return probability of the quantum walk. Another interesting quantity is the mean square distance $\text{MSD}(t)$. Let again be $|\langle i | \Psi(0) \rangle| = 1$, and let \mathbf{r}_j denote the Euclidean coordinates at any site j . The mean square distance is then defined as

$$\text{MSD}(t) = \sum_j |\mathbf{r}_j - \mathbf{r}_i|^2 |\langle j | \Psi(t) \rangle|^2. \quad (7)$$

Continuous-time classical random walk

With a proper choice of the on-site potentials ϵ_i , the Hamiltonian H also defines an analog classical evolution, cf. ref. 43. In the classical random walk, the probability of moving from site i to site j during a small time interval τ is given by $-\tau\langle j | H | i \rangle = \tau J$, for connected sites i and j . If i is connected to N_i different sites, the total probability of a move is τN_i . The probability of remaining on the site shall be given by $1 - \tau\langle i | H | i \rangle = 1 - \tau\epsilon_i$. To keep the probability normalized, we must have $\epsilon_i = N_i J$. On a Sierpiński gasket, $\epsilon_i = 4J$ for all sites, except for the three corner sites, where we have $\epsilon_i = 2J$. The definition of probabilities after an infinitesimal time step τ defines the probabilities for all times through a Schrödinger-like equation $\frac{d}{dt} p_{ji}(t) = -\sum_k \langle j | H | k \rangle p_{ki}(t)$. Under the boundary condition $p_{ji}(0) = \delta_{ji}$, with i denoting the site of initial preparation, the differential equation is solved by $p_{ji}(t) = \langle j | e^{-Ht} | i \rangle$. From this, we define the classical return probability $p_{ii}(t)$, or the mean square distance of the classical diffusive process by replacing $|\langle j | \Psi(t) \rangle|^2$ in Eq. (7) by $p_{ji}(t)$.

Data availability

Data will be made available upon reasonable request to the authors.

Code availability

Codes will be made available upon reasonable request to the authors.

Received: 14 February 2024; Accepted: 14 July 2024;

Published online: 02 August 2024

References

- Shang, J. et al. Assembling molecular Sierpiński triangle fractals. *Nat. Chem.* **7**, 389 (2015).
- Kempkes, S. N. et al. Design and characterization of electrons in a fractal geometry. *Nat. Phys.* **15**, 127 (2019).
- Xu, X.-Y., Wang, X.-W., Chen, D.-Y., Smith, C. M. & Jin, X.-M. Quantum transport in fractal networks. *Nat. Photon.* **15**, 703 (2021).
- Biesenthal, T. et al. Fractal photonic topological insulators. *Science* **376**, 1114 (2022).
- Tian, W. et al. Parallel assembly of arbitrary defect-free atom arrays with a multitweezer algorithm. *Phys. Rev. Appl.* **19**, 034048 (2023).
- Mandelbrot, B. How long is the coast of Britain? statistical self-similarity and fractional dimension. *Science* **156**, 636 (1967).
- Gefen, Y., Mandelbrot, B. B. & Aharony, A. Critical phenomena on fractal lattices. *Phys. Rev. Lett.* **45**, 855 (1980).
- Brzezińska, M., Cook, A. M. & Neupert, T. Topology in the Sierpiński-Hofstadter problem. *Phys. Rev. B* **98**, 205116 (2018).
- Pai, S. & Prem, A. Topological states on fractal lattices. *Phys. Rev. B* **100**, 155135 (2019).
- Iliosov, A. A., Katsnelson, M. I. & Yuan, S. Hall conductivity of a Sierpiński carpet. *Phys. Rev. B* **101**, 045413 (2020).
- Fremling, M., van Hooft, M., Smith, C. M. & Fritz, L. Existence of robust edge currents in Sierpiński fractals. *Phys. Rev. Res.* **2**, 013044 (2020).
- Manna, S., Nandy, S. & Roy, B. Higher-order topological phases on fractal lattices. *Phys. Rev. B* **105**, L201301 (2022).
- Ivaki, M. N., Sahlberg, I., Pöyhönen, K. & Ojanen, T. Topological random fractals. *Commun. Phys.* **5**, 327 (2022).
- Gefen, Y., Aharony, A., Mandelbrot, B. B. & Kirkpatrick, S. Solvable fractal family, and its possible relation to the backbone at percolation. *Phys. Rev. Lett.* **47**, 1771 (1981).
- Alexander, S. & Orbach, R. Density of states on fractals : fractons. *J. Phys. Lett.* **43**, 625 (1982).
- Rammal, R. & Toulouse, G. Random walks on fractal structures and percolation clusters. *J. Phys. Lett.* **44**, 13 (1982).
- Gefen, Y., Aharony, A. & Alexander, S. Anomalous diffusion on percolating clusters. *Phys. Rev. Lett.* **50**, 77 (1983).
- Havlin, S. & Ben-Avraham, D. Diffusion in disordered media. *Adv. Phys.* **36**, 695 (1987).
- Darázs, Z., Anishchenko, A., Kiss, T., Blumen, A. & Mülken, O. Transport properties of continuous-time quantum walks on Sierpiński fractals. *Phys. Rev. E* **90**, 032113 (2014).
- Kosior, A. & Sacha, K. Localization in random fractal lattices. *Phys. Rev. B* **95**, 104206 (2017).
- van Veen, E., Yuan, S., Katsnelson, M. I., Polini, M. & Tomadin, A. Quantum transport in Sierpiński carpets. *Phys. Rev. B* **93**, 115428 (2016).
- Gefen, Y., Aharony, A. & Mandelbrot, B. B. Phase transitions on fractals. iii. infinitely ramified lattices. *J. Phys. A: Math. Gen.* **17**, 1277 (1984).
- Domany, E., Alexander, S., Bensimon, D. & Kadanoff, L. P. Solutions to the Schrödinger equation on some fractal lattices. *Phys. Rev. B* **28**, 3110 (1983).
- Aubry, S. & André, G. Analyticity breaking and Anderson localization in incommensurate lattices. *Ann. Israel Phys. Soc.* **3**, 18 (1980).
- Kohmoto, M., Kadanoff, L. P. & Tang, C. Localization problem in one dimension: Mapping and escape. *Phys. Rev. Lett.* **50**, 1870 (1983).
- Anderson, P. W. Absence of diffusion in certain random lattices. *Phys. Rev.* **109**, 1492 (1958).
- Wang, X. R. Localization in fractal spaces: exact results on the Sierpiński gasket. *Phys. Rev. B* **51**, 9310 (1995).
- Tang, H. et al. Experimental two-dimensional quantum walk on a photonic chip. *Sci. Adv.* **4**, eaat3174 (2018).
- Razzoli, L., Paris, M. G. A. & Bordone, P. Continuous-time quantum walks on planar lattices and the role of the magnetic field. *Phys. Rev. A* **101**, 032336 (2020).
- Haake, F. *Quantum Signatures of Chaos* (Springer-Verlag, Berlin, Heidelberg, 2006)

31. Pal, B. & Saha, K. Flat bands in fractal-like geometry. *Phys. Rev. B* **97**, 195101 (2018).
32. Geisel, T., Ketzmerick, R. & Petschel, G. New class of level statistics in quantum systems with unbounded diffusion. *Phys. Rev. Lett.* **66**, 1651 (1991).
33. Sire, C., Passaro, B. & Benza, V. G. Electronic properties of 2d quasicrystals: level spacing distribution and diffusion. *J. Non-Crystalline Solids* **153-154**, 420 (1993).
34. Fleischmann, R., Geisel, T., Ketzmerick, R. & Petschel, G. Quantum diffusion, fractal spectra, and chaos in semiconductor microstructures. *Phys. D: Nonlinear Phenom.* **86**, 171 (1995).
35. Skinner, B., Ruhman, J. & Nahum, A. Measurement-induced phase transitions in the dynamics of entanglement. *Phys. Rev. X* **9**, 031009 (2019).
36. Yi, H. Quantum critical behavior of the quantum ising model on fractal lattices. *Phys. Rev. E* **91**, 012118 (2015).
37. Xu, Y.-L., Kong, X.-M., Liu, Z.-Q. & Yin, C.-C. Scaling of entanglement during the quantum phase transition for ising spin systems on triangular and sierpiński fractal lattices. *Phys. Rev. A* **95**, 042327 (2017).
38. Krcmar, R. et al. Tensor-network study of a quantum phase transition on the sierpiński fractal. *Phys. Rev. E* **98**, 062114 (2018).
39. Manna, S., Pal, B., Wang, W. & Nielsen, A. E. B. Anyons and fractional quantum Hall effect in fractal dimensions. *Phys. Rev. Res.* **2**, 023401 (2020).
40. Manna, S., Duncan, C. W., Weidner, C. A., Sherson, J. F. & Nielsen, A. E. B. Anyon braiding on a fractal lattice with a local Hamiltonian. *Phys. Rev. A* **105**, L021302 (2022).
41. Li, X., Jha, M. C. & Nielsen, A. E. B. Laughlin topology on fractal lattices without area law entanglement. *Phys. Rev. B* **105**, 085152 (2022).
42. Koch, G. & Posazhennikova, A. Loop current states and their stability in small fractal lattices of bose-einstein condensates (2024), <https://arxiv.org/abs/2401.08393> [cond-mat.quant-gas].
43. Farhi, E. & Gutmann, S. Quantum computation and decision trees. *Phys. Rev. A* **58**, 915 (1998).

Acknowledgements

T.G. acknowledges funding by Gipuzkoa Provincial Council (QUAN-000021-01), by the Department of Education of the Basque Government through the IKUR strategy and through the project PIBA_2023_1_0021 (TENINT), by the Agencia Estatal de Investigación (AEI) through Proyectos de Generación de Conocimiento PID2022-142308NA-I00 (EXQUSMI), and that this work has been produced with the support of a 2023 Leonardo Grant for Researchers in Physics, BBVA Foundation. The BBVA Foundation is not responsible for the opinions, comments and contents included in the project and/or the results derived therefrom, which are the total and absolute responsibility of the authors. B.J.-D. and A.R.-F. acknowledge funding from Grant No. PID2020-114626GB-I00 by MCIN/AEI/10.13039/5011 00011033 and "Unit of Excellence María de Maeztu 2020–2023" award to the Institute of Cosmos Sciences, Grant CEX2019-000918-M funded by MCIN/AEI/10.13039/501100011033. We acknowledge financial support from the Generalitat de Catalunya (Grant 2021SGR01095). A.R.-F. acknowledges funding from MIU through Grant No. FPU20/06174. U.B. acknowledges support from: ERC AdG NOQIA; MCIN/AEI (PGC2018-0910.13039/501100011033, CEX2019-000910-S/10.13039/501100011033, Plan National FIDEUA PID2019-106901GB-I00, Plan National STAMEENA PID2022-139099NB-I00 project funded by MCIN/AEI/10.13039/501100011033 and by the "European Union NextGenerationEU/PRTR" (PRTRC17.11), FPI); QUANTERA MAQS PCI2019-111828- 2; QUANTERA DYNAMITE PCI2022-132919 (QuantERA II Programme co-funded by European Union's Horizon 2020 program under Grant Agreement No 101017733), Ministry of Economic Affairs and Digital Transformation of the

Spanish Government through the QUANTUM ENIA project call - Quantum Spain project, and by the European Union through the Recovery, Transformation, and Resilience Plan - NextGenerationEU within the framework of the Digital Spain 2026 Agenda; Fundació Cellex; Fundació Mir-Puig; Generalitat de Catalunya (European Social Fund FEDER and CERCA program, AGAUR Grant No. 2021 SGR 01452, QuantumCAT U16-011424, co-funded by ERDF Operational Program of Catalonia 2014-2020); Barcelona Supercomputing Center MareNostrum (FI-2023-1-0013); EU Quantum Flagship (PASQuanS2.1, 101113690); EU Horizon 2020 FET-OPEN OPTologic (Grant No 899794); EU Horizon Europe Program (Grant Agreement 101080086 — NeQST), ICFO Internal "QuantumGaudi" project; European Union's Horizon 2020 program under the Marie Skłodowska-Curie grant agreement No 847648; "La Caixa" Junior Leaders fellowships, La Caixa" Foundation (ID 100010434): CF/BQ/PR23/11980043. Views and opinions expressed are, however, those of the author(s) only and do not necessarily reflect those of the European Union, European Commission, European Climate, Infrastructure and Environment Executive Agency (CINEA), or any other granting authority. Neither the European Union nor any granting authority can be held responsible for them. U.B. is also grateful for the financial support of the IBM Quantum Researcher Program.

Author contributions

T.G. conceived and supervised the project. A.R.-F., P.P., and T.G. developed the codes and performed numerical simulations. A.R.-F., B.J.-D., T.G., and U.B. analyzed and interpreted the data. A.R.-F. and T.G. wrote the manuscript with the feedback from all co-authors.

Competing interests

The authors declare no competing interests.

Additional information

Supplementary information The online version contains supplementary material available at <https://doi.org/10.1038/s42005-024-01747-x>.

Correspondence and requests for materials should be addressed to Tobias Grass.

Peer review information *Communications Physics* thanks the anonymous reviewers for their contribution to the peer review of this work. A peer review file is available.

Reprints and permissions information is available at <http://www.nature.com/reprints>

Publisher's note Springer Nature remains neutral with regard to jurisdictional claims in published maps and institutional affiliations.

Open Access This article is licensed under a Creative Commons Attribution 4.0 International License, which permits use, sharing, adaptation, distribution and reproduction in any medium or format, as long as you give appropriate credit to the original author(s) and the source, provide a link to the Creative Commons licence, and indicate if changes were made. The images or other third party material in this article are included in the article's Creative Commons licence, unless indicated otherwise in a credit line to the material. If material is not included in the article's Creative Commons licence and your intended use is not permitted by statutory regulation or exceeds the permitted use, you will need to obtain permission directly from the copyright holder. To view a copy of this licence, visit <http://creativecommons.org/licenses/by/4.0/>.

© The Author(s) 2024